Journal of Molecular Catalysis A: Chemical 340 (2011) 39–47

Contents lists available at ScienceDirect

Journal of Molecular Catalysis A: Chemical

journal homepage: www.elsevier.com/locate/molcata

Effect of Re addition on the activities of Co/CeO_2 catalysts for water gas shift reaction

Kingkaew Chayakul, Tipaporn Srithanratana, Sunantha Hengrasmee*

Department of Chemistry and Center of Excellence for Innovation in Chemistry, Faculty of Science, Khon Kaen University, Khon Kaen 40002, Thailand

ARTICLE INFO

Article history:
Received 11 October 2010
Received in revised form 9 February 2011
Accepted 9 March 2011
Available online 15 March 2011

Keywords:
Re–Co bimetallic catalyst
X-ray absorption near edge structure
Water gas shift reaction
Oxygen vacancies

ABSTRACT

The catalytic activities of $Re–Co/CeO_2$ bimetallic catalysts for the water gas shift (WGS) reaction were investigated and compared with activities of Co/CeO_2. It was found that the rate of WGS reaction over $Re–Co/CeO_2$ bimetallic catalysts was higher than that of a single catalyst of Co on ceria. It seems that Re influences the catalysts and the catalyst performance in several ways. XRD and Raman spectroscopy results indicate that metal oxides were dispersed on ceria surface and H_2-chemisorption indicated better dispersion of Co on the ceria surface upon addition of Re. X-ray absorption near edge structure (XANES) spectra of $Re–Co/CeO_2$ indicate that Re promotes the reduction of surface ceria to Ce_2O_3 and provides oxygen vacancies that facilitate the redox process at the surface. XANES also indicated that electron densities were withdrawn from Co d-state to Re, leading to weaker Co-adsorbate bonds. All of these effects contribute to an increase in the WGS reaction rate.

1. Introduction

The water gas shift (WGS) reaction is an important step in reducing the amount of CO from H_2 feed gas that will be used in fuel cells. H_2 feed gas is obtained as the major product of a reforming reaction together with a small amount of by-products such as CH_4, H_2O, and CO. Among these impurities, CO is poisonous to the Pt electrode in a PEM fuel cell and decreases Pt activity. Removal of CO from the feed gas is necessary, and the water gas shift reaction which can reduce the amount of CO to less than 0.5–1% is a candidate for this step.

In the WGS reaction, carbon monoxide is converted to carbon dioxide by water vapor. The WGS reaction is described by the following reaction,

$$CO + H_2O \rightleftharpoons CO_2 + H_2 \qquad \Delta H = -41.2\,kJ/mol$$

This reaction is exothermic and the rate equilibrium conversion is lower with increasing temperature. In order to keep good conversion rates at low temperature, catalysts must be employed.

The catalysts that are widely used are metal–ceria based catalysts [1–6]. Ceria (CeO_2) is a suitable support due to its high oxygen storage capacity, high reducibility and high oxygen mobility [7–11]. Many precious metals such as Pt, Pd, Rh, Ru and Au have been reported to show high WGS reaction rate when they are doped on ceria supports [12–21]. Among these metals, Pt and Au which are rare and expensive are the most promising promoters because of their better catalytic activity at low temperature. Many research groups are trying to develop new types of catalysts from metals that are less expensive and more abundant. Many studies have shown that a combination of two metals can provide rather good WGS activities. Many bimetallic systems have been studied for many reactions, for example $Pt–V/CeO_2$, $Pt–Re/CeO_2–ZrO_2$ and Au–M on iron(III) oxide (M = Ag, Bi, Co, Cu, Mn, Ni, Pb, Ru, Sn and Tl) have been found to increase the rates of WGS reactions [22–26], while $Pt–Sn/Nb_2O_5$ is also active for selective CO-oxidation [27,28]. Among the second metals that have been used to form bimetallic catalysts, Re is the most widely studied. Apart from increasing the WGS rate, Pt–Re/carbon has also been reported to be active for many other reactions such as hydrocarbon reforming [29] and conversion of glycerol to synthesis gas [30]. Our initial investigation found that Re also increased the rate of WGS reaction when it was doped on Co/CeO_2.

The manner in which Re improves the catalytic performance varies. For the WGS reaction, Choung et al. [23] indicated that the effect was partly due to better dispersion of Pt on the support, but the actual role was more complex. Iida and Igarashi [25], in comparing the rate of WGS reaction of $Pt–Re/TiO_2$ (rutile) and $Pt–Re/ZrO_2$, indicated that the effect of Re on Pt dispersion and catalytic activity was largely affected by the state of the Re. In a recent paper on conversion of glycerol by Pt–Re catalysts [30], Re was reported to participate in weakening the binding energy of CO to the neighboring Pt sites. X-ray absorption spectroscopy was employed to study the oxidation state of Re and Pt. Hilbrig et al. [31] demonstrated that X-ray absorption near edge structure (XANES) can be used to determine the degree of reduction/interaction of bimetallic catalysts and

* Corresponding author. Tel.: +66 43202222x12243; fax: +66 43202373.
E-mail address: sunhen@kku.ac.th (S. Hengrasmee).

1381-1169/$ – see front matter © 2011 Elsevier B.V. All rights reserved.
doi:10.1016/j.molcata.2011.03.006

reported XANES-TPR studies of Pt–Re/Al_2O_3 and silica-supported Pt/Ni catalysts [31,32]. Apart from identifying the binding energies and oxidation state, XANES can also indicate changes in electron density of the metal d-band. Study of Pd L_3 near-edge absorption in Ag-promoted Pd catalyst indicated increases in the Pd d-band electron densities upon addition of Ag [33]. Pereira et al. [34] used XANES to study bonding of CO on Pt-based bimetallic catalysts and found increases of Pt 5d-band vacancies for Pt–M/C bimetallic catalysts, which indicated a lowering of electron back-donation to the CO molecules. In studying the activity of Re–Co/alumina in the Fischer–Tropsch reaction, Re was reported to be a reduction promoter that facilitated the rate of reduction of cobalt species interacting with the support and generated more available active cobalt metal sites to participate in the reaction [35].

In WGS reaction, the oxidation–reduction process is one of the rate limiting steps that control the reaction rate. Many studies reported that the reducible support (CeO_2, ZrO_2, TiO_2, etc.) is usually used due to its participation in enhancing the WGS reaction. CeO_2 can store and release oxygen to undergo oxidation–reduction cycles and promote catalytic activity for this reaction. Several studies have reported that metal-modified ceria has a higher oxygen storage capacity and reducibility than pure ceria [36–38]. Sanchez and Gazquez [39] proposed that oxygen vacancies in the fluorite structure of the supported catalysts alter the morphology and dispersion of the supported metal. In an attempt to dope Pt/CeO_2 catalysts with many metal cations, Panagiotopoulou and co-worker [40] reported that the WGS activities of Pt/Ce–Me–O catalysts (Me = metal cations) depended on the nature of the dopants employed and the promotions affected the reducibility and oxygen ion mobility of the CeO_2 support. Creation of oxygen vacancies lead to an improvement of oxygen mobility from the support to the adsorbed species on the catalyst surface.

In this paper, we report the enhancement of WGS reaction rate when Re is doped to Co/ceria catalysts. The catalysts were prepared by the incipient-wetness impregnation method and characterized by X-ray diffraction (XRD), N_2-adsorption, H_2-chemisorption, Raman spectroscopy and H_2-temperature programmed reduction (H_2-TPR). XANES of the catalysts was employed to investigate the movement of metal d-electrons in the catalysts.

2. Experimental

2.1. Catalysts preparation

2.1.1. Preparation of support

CeO_2 support was prepared by the urea gelation method which was similar to the process described by Kundakovic and Flytzani-Stephanopoulos [5] and Bickford et al. [41]. An appropriate amount of cerium nitrate hexahydrate ($Ce(NO_3)_3{\cdot}6H_2O$, 99%, Aldrich) and 12 g of urea (H_2NCONH_2, 98%, Aldrich) were dissolved in 100 mL of deionized water. The mixture was stirred and heated at 100–120 °C until the salts were dissolved. While the mixture was heated, 2 mL of ammonium hydroxide (NH_4OH, Aldrich) was added dropwise to obtain a yellow precipitate. The suspension was heated and stirred for 4 h to remove excess ammonia and to age the support. After aging, the precipitate was filtered and washed with boiling deionized water. The filtered support was dried overnight at 110 °C in a furnace and calcined at 450 °C for 4 h.

2.1.2. Preparation of catalysts

The incipient wetness impregnation method with a minimum amount of solvent was used to prepare the catalysts. The desired amounts of ammonium perrhenate (NH_4ReO_4, 99%, Aldrich) and cobalt(II)nitrate hexahydrate ($Co(NO_3)_2{\cdot}6H_2O$, 98%, Carlo Erba) were dissolved in a minimal amount of deionized water. The solution was added dropwise to the prepared CeO_2 support. The impregnated supports were dried at 110 °C overnight and calcined at 650 °C for 8 h.

2.2. Catalyst characterization

2.2.1. Standard characterization

XRD patterns of ceria based catalysts and all doped metal–ceria based catalysts were obtained from Bruker XRD D8 Advance GX 280 with Cu K_α radiation of wavelength 1.5406 Å. The diffractograms were recorded in the range of 2θ = 20–80° with a scan speed of 0.5 s per step. The crystalline sizes of the samples, d_{hkl}, were estimated from Scherrer's equation

$$d_{hkl} = \frac{0.9\lambda}{\mathrm{FWHM}\ \cos\theta} \quad (1)$$

where λ is the X-ray wavelength of Cu K_α radiation (1.5406 Å), FWHM is the broadening (in radians) at half-maximum of the (1 1 1) crystallographic plane which is the most intense peak and θ is the diffraction angle corresponding to the (1 1 1) plane. Lattice parameter (a) is calculated by Bragg's equation with the same crystallographic plane.

The specific surface areas of the catalysts were obtained from the N_2 adsorption isotherm at 77 K using the Brunauer Emmett Teller (BET) method by Quantachrome Autosorb 1-C instrument. The catalysts were degassed at 300 °C for 3 h prior to an adsorption experiment. The specific surface area was calculated by the multipoint-BET method and the average pore volume and diameter were determined at relative pressure $P/P_0 \sim 0.99$.

H_2-chemisorption of all catalysts was studied by Quantachrome Autosorb 1-C instrument. The catalysts were first pretreated by Helium at 120 °C (rate 20 °C/min) for 30 min, then H_2 (99.999%, Thai Industrial Gas) was flowed over the sample while the temperature was raised at the rate of 20 °C/min to reach 350 °C and was held at this temperature for 120 min. After sample preparation, the sample was cooled down under vacuum to room temperature (40 °C). The adsorbing gas (H_2) was sequentially added to the sample. An adsorbed volume (V) vs. Equilibrium pressure (P/P_0) isotherm was generated. The H_2 chemisorbed and the percentage of metal dispersion can be deduced from this chemisorbed isotherm. The method used to obtain the volume of monolayer uptake (V_m) is an extrapolation method. The monolayer of hydrogen uptake (N_m) is expressed in μmol of hydrogen per gram of sample, that is

$$N_m = 44.61 V_m \quad (2)$$

where V_m (cc/g) is determined by extrapolating the isotherm to zero pressure. The percent metal dispersion (D) can be estimated from the equation

$$D = \frac{N_m S M}{100 L} \quad (3)$$

where S is the adsorption stoichiometry of H_2 which is equal to 2, M and L are the molecular weight of loading metal and percent loading of the supported metal, respectively.

2.2.2. Raman spectroscopy

The Raman spectra of all catalysts were recorded by Jobin Yvon T 64000 Raman spectrometer equipped with BX51 Olympus optical microscope. The Raman spectrometer was used to observe the vibrational mode of prepared catalyst powder and the vibrational signal was detected by Charge Coupled Device (CCD) detector. The samples were irradiated by Ar ion laser with an output power 30 mW and wavelength of 514.532 nm. The Raman spectra were collected in the range of 200–2000 cm^{-1}.

2.2.3. H_2-temperature programmed reduction (H_2-TPR)

H_2-TPR was carried out using the Quantachrom Autosorb 1-C instrument. The samples were pretreated by helium at 120 °C (rate 10 °C/min) for 30 min. After cooling down to room temperature, a gaseous mixture of 5%H_2 in 95%N_2 was flowed over the pretreated sample while the temperature was increased from 40 °C to 1000 °C at a rate of 10 °C/min. The products were analyzed with TCD detector and H_2-consumption was plotted as a function of temperature.

2.3. Water gas shift catalytic activity test

WGS catalytic activities of all samples were tested with a flow reactor in the temperature range of 150–600 °C. 20 mg of catalysts were packed and sandwiched between two layers of quartz wool in the quartz tube reactor with 0.6 cm ID, 0.8 cm OD × 30 cm length. The quartz tube was placed inside the temperature controllable tube furnace. The temperature was monitored by K-type thermocouple that was placed at the top of the catalyst bed. The flow of feed gases was controlled by mass flow controllers (Dywer). Both temperature and flow rate were monitored by Data Logger Wisco DL2100B. The initial feed gas, consisting of CO and He at a flow rate of 5 and 85 mL/min respectively, was flowed into a water-saturator in which the temperature was kept at 47 °C to pick up water vapor. The mixed feed gas containing 5%CO, 10%H_2O and 85%He, was allowed to pass through the catalyst bed of the reactor. The reactants and products were analyzed by on-line gas chromatography (Agilent 6890N Series, Agilent Technology) equipped with HEYSEP D Packed Column and TCD detector. The percentage conversion of CO was plotted as a function of temperature.

The rates of reaction were obtained from separate experiments under differential conditions, where the conversions of reactants were lower than 10% and with this condition heat and mass transfer effects were negligible. The rates were calculated by the following expression

$$r_{CO} = \frac{F_{CO} \times X_{CO}}{W_{cat}} \quad (4)$$

where r_{co} is the conversion rate of CO (mol g^{-1} s^{-1}), F_{co} is the molar flow rate of CO (mol s^{-1}), W_{cat} is the mass of the catalysts (g) and X_{co} is the conversion of CO which is defined as

$$X_{CO} = \frac{C_{CO}^{in} - C_{CO}^{out}}{C_{CO}^{in}} \quad (5)$$

The r_{co} reported in this manuscript is an average of three reproducible experiments.

2.4. X-ray adsorption near edge structure

X-ray absorption spectroscopy (XAS) measurements were studied in the XANES region on Beamline 8 [42] at the Synchrotron Light Research Institute (SLRI), Nakhon Ratchasima, Thailand. The measurements were carried out in fluorescence mode for Re M_5 and Co K absorption edges and transmission modes for Ce L_3 absorption edge. Synchrotron radiation is tunable by a fixed-exit double crystal monochromator (DCM) equipped with InSb(1 1 1) and Ge(2 2 0) crystals for low and high energy ranges, respectively. The monochromatic flux at the sample was 10^8–10^{10} phs/s. The samples were deposited over the Kapton window which was placed on the sample frame. Ion chambers were filled with a mixture of nitrogen and helium for Re M_5 absorption measurement and with argon and helium for Ce L_3 and Co K absorption edge measurements. These chambers were installed in front of and behind the sample which continuously detected the incident (I_o) and transmitted (I_1) X-ray beams. A Lytle detector was used to detect sample fluorescence. The software Athena was used to process the data reduction. Data reduction was carried out by pre-edge background removal and normalization by division of the height of the adsorption edge.

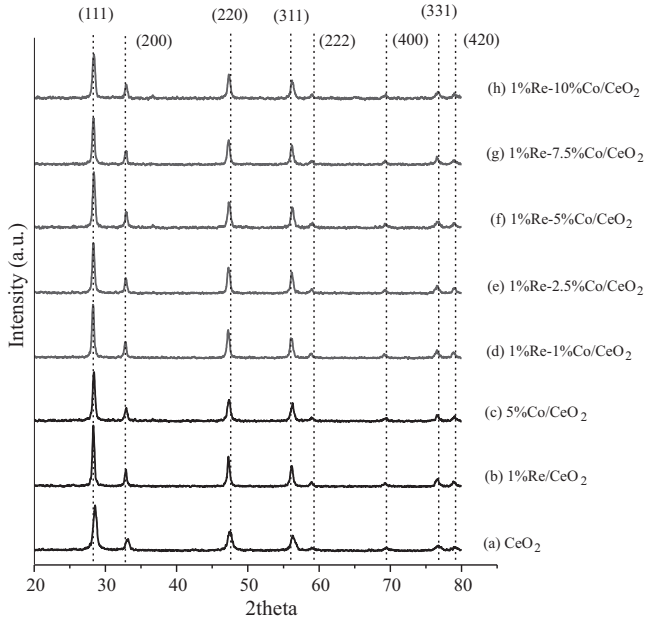

Fig. 1. XRD patterns of (a) CeO_2, (b) 1%Re/CeO_2, (c) 5%Co/CeO_2 and (d)–(h) 1%Re–*X*%Co/CeO_2 (*X* = 1.0, 2.5, 5.0, 7.5 and 10.0) catalysts.

3. Results and discussion

3.1. Standard characterization

XRD patterns of CeO_2, Co/CeO_2 monometallic and Re–Co/CeO_2 bimetallic catalysts are shown in Fig. 1. All of these samples exhibit diffraction peaks which correspond to the fluorite type structure of CeO_2. Neither Re nor Co oxide phases were observed in all spectra. This suggests that the metal oxide species were highly dispersed on the ceria surface [43,44].

The lattice parameters of ceria and metal–ceria based catalysts were calculated by (1 1 1) crystallographic planes which are based on Bragg's equation. For pure CeO_2 support, the lattice parameter is 0.541 nm which is in agreement with other works [40,45]. The lattice parameter of other catalysts (Co/CeO_2, and Re–Co/CeO_2) also displayed similar values varying from 0.544 to 0.547 nm. It can be concluded that addition of Co or Re did not lead to modification of crystal structures.

The results from particle analysis together with the XRD results are summarized in Table 1. Increases in crystalline sizes were observed for all samples of doped ceria. This result is suggested to be due to agglomeration and growth of metal–ceria crystallites after calcination at high temperature [46]. The BET surface area of CeO_2 is 68.3 m^2/g which is in agreement with others [5,36,47]. Introduction of metals onto the ceria surface by the impregnation method led to particle pore blocking and gave rise to lowering of surface area and pore volume and consequently the pore diameter was enlarged.

The results from H_2-chemisorption and % active metal dispersion are also displayed in Table 1. H_2 was not chemisorbed on Re and the data on H_2-chemisorption and % active metal dispersion are referred to Co metal. The% metal dispersion data indicate that Re helped to disperse Co metal on ceria support. However, the dispersion decreased with an increase of Co. This result, as also indicated by XRD, was due to agglomeration and the growth of

Table 1
Specific surface area, crystalline size, lattice constant, H_2 chemisorbed and % dispersion of various catalysts.

Sample	S_{BET} (m^2/g)	Crystalline size[a] (nm)	Lattice constant[a] (nm)	H_2 chemisorbed (μmol/g)	% dispersion
CeO_2	68.3	14.2	0.541	–	–
1%Re/CeO_2	26.8	22.6	0.545	–	–
5%Co/CeO_2	28.0	21.6	0.544	39.1	9.2
1%Re–1%Co/CeO_2	22.9	23.5	0.547	45.2	53
1%Re–2.5%Co/CeO_2	26.9	19.5	0.544	46.0	22
1%Re–5%Co/CeO_2	22.9	21.5	0.545	45.3	11
1%Re–7.5%Co/CeO_2	25.3	26.0	0.545	45.5	7.2
1%Re–10%Co/CeO_2	22.9	19.0	0.544	46.6	5.5

[a] Calculated from the (1 1 1) crystallographic plane.

metal–ceria crystallites. As the result of better metal dispersion, the H_2-chemisorption increased.

3.2. Raman spectroscopy

Raman spectroscopy is a powerful technique sensitive to observing M–O bond arrangement and lattice defects [48]. Ceria with fluorite structure (space group F_{m3m}) has a very simple vibration structure with only one Raman active mode. The Raman spectra of pure CeO_2 displays only one prominent peak at 464 cm^{-1} due to F_{2g} Raman active mode of the fluorite structure [49] as shown in Fig. 2. This vibration mode is a symmetric breathing mode of 8 oxygen atoms around each Ce cation. Incorporation of some ions of similar size but different charges into the CeO_2 lattice would lead to shifting and lowering of the intensity of the 464 cm^{-1} peak, along with the appearance of a small additional peak due to vibration of oxygen around the added atom, and these phenomena indicate the existence of oxygen vacancies [50].

In studying the Raman spectra of cobalt oxide on γ-alumina, Zacharaki et al. [51] reported 5 characteristic bands due to the crystalline Co_3O_4 spinel with Co^{2+} and Co^{3+} located at tetrahedral and octahedral sites, respectively. These bands were identified as A_{1g} (694 cm^{-1}), F_{2g} (622 cm^{-1}), F_{2g} (527 cm^{-1}), E_g (487 cm^{-1}) and F_{2g} (198 cm^{-1}).

In our Raman spectra, the 464 cm^{-1} band was assigned to Ce–O vibration and other peaks were assigned to the existence of small crystallites of Co_3O_4 which are present at the surface of CeO_2. The occurrence of the CoO phase may also be possible since the 484 and 691 cm^{-1} CoO bands coincide with the Co_3O_4 band [52]. The Re–O vibration band was not observed due to very low Re content. Upon investigating the 464 cm^{-1} band of CeO_2, it is clearly seen that the addition of Re or Co did not lead to additional peak of other metal oxide species and this result indicates the preservation of the bulk structure. However, the intensities of the 464 cm^{-1} band were gradually lowered and a slight red shift of 2–3 cm^{-1} was observed with the increase of the added metals. This result may due to the presence of Ce^{3+}at the catalyst surface which is produced upon reduction of surface Ce^{4+} by Co and by Re.

3.3. H_2-temperature programmed reduction

H_2-TPR profiles of ceria, monometallic (Re/CeO_2 and Co/CeO_2) and bimetallic catalysts (Re–Co/CeO_2) are presented in Fig. 3. For CeO_2, there are two main reduction peaks at 520 and 880 °C which are attributed to reduction of the uppermost layer of Ce^{4+} in CeO_2 and the main peak at high temperature is assigned to the reduction of bulk ceria [53]. Addition of Re or Co onto CeO_2 brought up additional reduction peaks around 300–380 °C. In the case of Re/CeO_2, two reduction peaks were observed. The first one is located at 300 °C and the other at 530 °C. The lower temperature reduction peak is attributed to reduction of rhenium oxide species [54], and

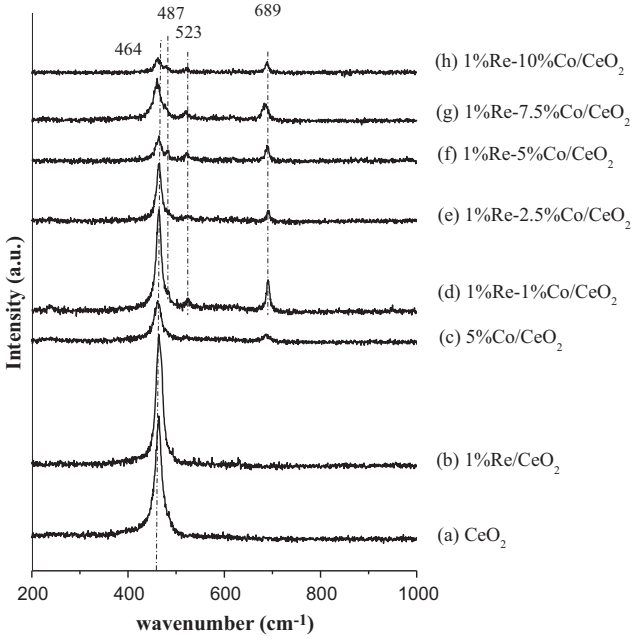

Fig. 2. Raman spectra of (a) CeO_2, (b) 1%Re/CeO_2, (c) 5%Co/CeO_2 and (d)–(h) 1%Re–*X*%Co/CeO_2 (*X* = 1.0, 2.5, 5.0, 7.5 and 10.0) catalysts.

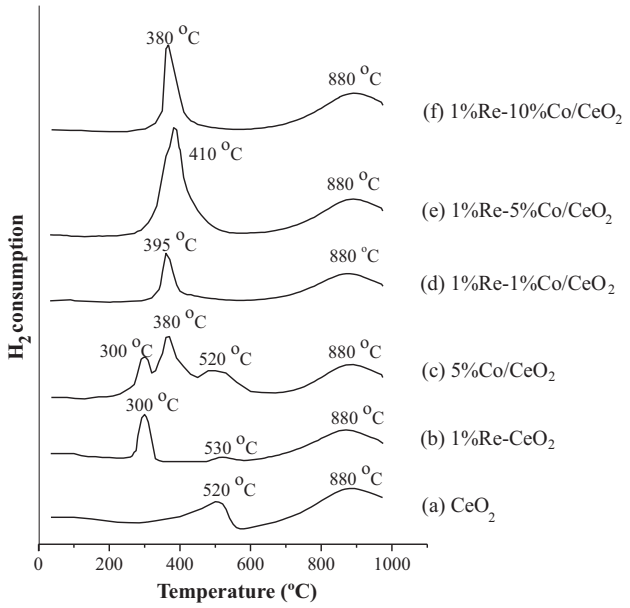

Fig. 3. H_2-TPR profiles of (a) CeO_2, (b) 1%Re/CeO_2, (c) 5%Co/CeO_2 and (d)–(f) 1%Re–*X*%Co/CeO_2 (*X* = 1.0, 5.0 and 10.0) catalysts.

the peak at 530 °C is due to CeO_2. It is not clear what the final state of Re is after the reduction, since it seems to depend on the state of the supports. For examples, Johnson and LeRoy [55] reported that rhenium on alumina is reduced exclusively by hydrogen to the Re^{4+} state. In contrast, Webb [56] reported that alumina supported rhenium is completely reduced at 400 °C. Jacobs et al. [35], upon studying Re–Co/Al_2O_3, reported that Re promoted the reduction of CoO to Co^0, and Re remains on the surface as isolated Re atoms in intimate contact with Co metal clusters. Extensive study is required in order to determine the final state of Re/CeO_2 upon hydrogen reduction. For Co/CeO_2, two additional peaks at 300 and 380 °C point to a two-step reduction process of cobalt oxide ($Co^{3+} \rightarrow Co^{2+} \rightarrow Co^0$). Luo et al. [57] reported the reduction of Co^{3+} at the interface between Co_3O_4 and CeO_2 to Co^{2+} in the temperature range of 240–320 °C and the reduction of Co_3O_4 that weakly interacts with CeO_2 to Co in the range of 320–480 °C. Variations of TPR spectra of Co/CeO_2 have been reported [58–60] and the differences of the spectra have been discussed to be due to various factors such as precursor salts and treatment conditions. Our results seem to agree with the results of Luo et al. [57]. The existence of reduction peaks of metal oxides that are separated from CeO_2 reduction peaks indicates that these oxide phases are separate and probably reside on the surface of ceria, leading to a weaker surface ceria signal.

The H_2-TPR of the bimetallic catalysts Re–Co/CeO_2 are different from those of monometallic catalysts. In this case the surface reduction temperature of ceria at 520 °C disappears and a concurrent reduction of metal oxide species appears as a broad peak ranging from 300 to 480 °C with peak center situated around 380–410 °C. Electron density transfer between Re, Co, and Ce may occur. As the result of electron density transfer, reduction of the catalyst surface is easier.

3.4. Water gas shift catalytic activity

The WGS catalytic activities of 5%Co/CeO_2 monometallic and 1%Re–*X*%Co/CeO_2 bimetallic catalysts are presented in Fig. 4(a), where the conversion of CO is plotted as a function of temperature. It was found that doping 1% of Re onto Co/CeO_2 with various loading of Co to form bimetallic catalysts result in shifts of the conversion curves toward a lower reaction temperature (lines b–f) compared with that of Co on ceria (line a). The Re–Co/CeO_2 bimetallic catalysts exhibit higher CO conversion rate compared to the monometallic one, which become active at temperatures higher than 220 °C while X_{co} increases with increasing temperature and reaches equilibrium conversion around 390 °C. The effect of Co loading on catalytic activities is also illustrated in Fig. 4(a). It is found that further increases of Co content do not shift the conversion curve toward lower temperature (lines b–f). 1%Re–5%Co/CeO_2 is the most active catalyst at this condition and gives measurable conversion at temperatures lower than 250 °C. The WGS activity of 1%Re/CeO_2 was plotted for comparison (line a) and it is clearly seen that 1%Re/CeO_2 is not very active for the WGS reaction.

The Arrhenius plots of monometallic and bimetallic catalysts are illustrated in Fig. 4(b). These plots also display that the rate of CO conversion of bimetallic catalyst is higher than the rate of monometallic catalysts. Table 2 summarizes the rate of WGS reaction and apparent activation energies which are obtained from the slope of the Arrhenius plot. The rates (per gram of catalyst) of Re–Co/CeO_2 bimetallic catalysts are very much higher than those of Co/CeO_2. For example, the WGS rate upon 1%Re–5%Co/CeO_2 is 33.9 μmol/g s while the rate on 5%Co/CeO_2 is only 3.83 μmol/g s. Further addition of Re does not further raise the rate of the reaction and the appropriate amount of Re that is enough to maximize the WGS rate is 1 weight percent. When attention is drawn to the variation of Co content, it appears that the bimetallic catalyst with

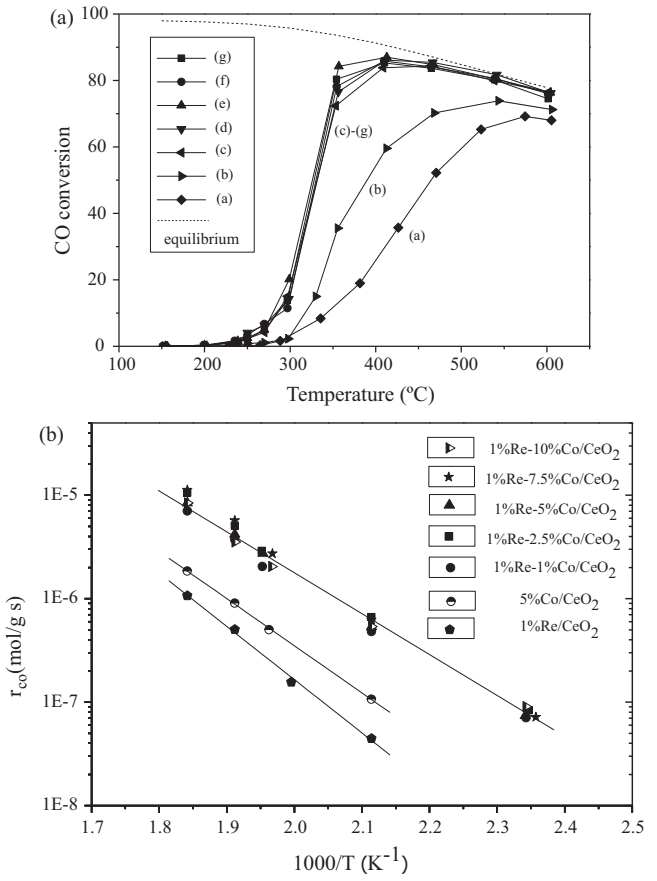

Fig. 4. (a) WGS catalytic activities of (a) 1%Re/CeO_2, (b) 5%Co/CeO_2, and (c)–(g) 1%Re–*X*%Co/CeO_2 (*X* = 1.0, 2.5, 5.0, 7.5 and 10.0) catalysts. (b) Arrhenius plot of reaction rates over 1%Re/CeO_2, 5%Co/CeO_2 and 1%Re–*X*%Co/CeO_2 (*X* = 1.0, 2.5, 5.0, 7.5 and 10.0) catalysts.

1%Re and 5%Co gives the highest WGS rate under this working condition. Lowering of the apparent activation energy is also observed. For reaction on 5%Co/CeO_2 the activation energy is 84 kJ/mol while the activation energies of bimetallic catalysts are between 76 and 80 kJ/mol. These values do not vary with variation of Co or Re contents which could indicate that under these experimental conditions, the rate limiting step is not affected by variation of Co or Re contents. Other parameters that did not change with the increase of metal contents are surface area and H_2-chemisorption (Table 1). This result indicates that the WGS reaction activity depends on the physical state of the catalyst and not on the metal contents. The calculated values of E_a are in agreement with those reported for various metals on ceria supports [40,61,62].

Table 2
The rate of reaction at 290 °C and apparent activation energy (E_a) for all doped catalysts.

Sample	Rate at 290 °C (μmol/g s)	E_a (kJ/mol)
5%Co/CeO_2	3.83	84
1%Re/CeO_2	2.80	90
1%Re–5%Co/CeO_2	33.9	76
2%Re–5%Co/CeO_2	30.8	77
5%Re–5%Co/CeO_2	32.4	79
1%Re–1%Co/CeO_2	25.3	77
1%Re–2.5%Co/CeO_2	23.9	77
1%Re–5%Co/CeO_2	33.9	76
1%Re–7.5%Co/CeO_2	21.3	80
1%Re–10%Co/CeO_2	23.0	77

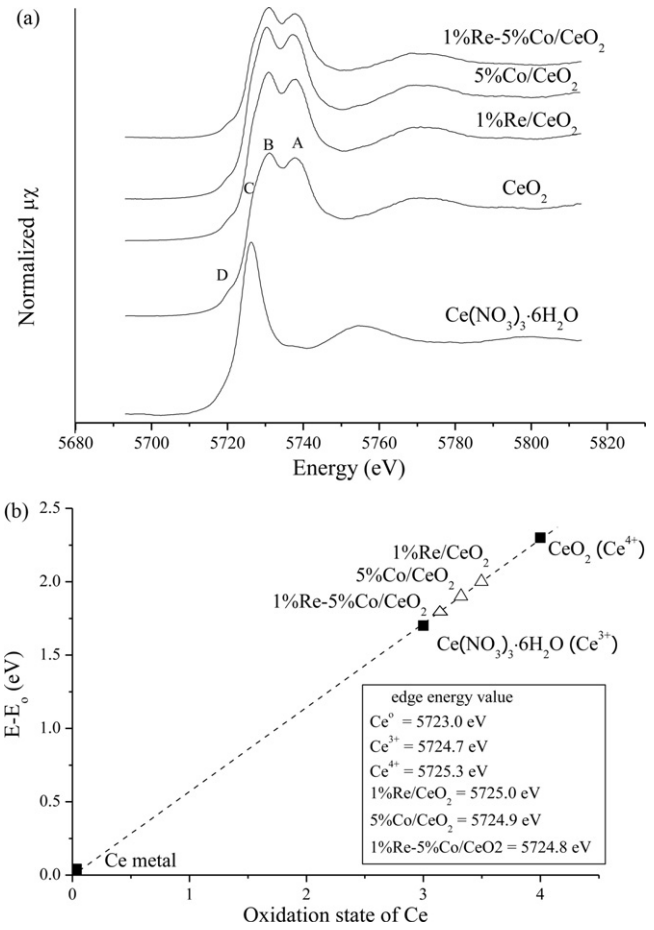

Fig. 5. (a) XANES spectra of the Ce L_3 absorption edge for $Ce(NO_3)_3{\cdot}6H_2O$ (Ce^{3+}), CeO_2 (Ce^{4+}), 1%Re/CeO_2, 5%Co/CeO_2 and 1%Re–5%Co/CeO_2. (b) Relationship between edge energy shift of Ce compounds and the oxidation states. Filled squares are Ce^0, $Ce(NO_3)_3{\cdot}6H_2O$ (Ce^{3+}) and CeO_2 (Ce^{4+}) standards, open triangles are 1%Re/CeO_2, 5%Co/CeO_2 and 1%Re–5%Co/CeO_2.

3.5. X-ray absorption spectroscopy

It is interesting to try to understand the role of Re in enhancing the WGS activity of Co on ceria. The results from the H_2-TPR study indicate that the catalyst surfaces were easier to reduce at temperatures lower than the surface reduction temperature of ceria when the catalysts were doped with 1%Re. Since the reduction process involves electron transfer among the involved species, it is interesting to study the electron movement within the catalyst surfaces and XAS was employed to study the electronic nature of our catalysts. In the XAS technique, an intense X-ray beam is used to excite core electrons of atoms at the surface to the unoccupied valence shell. The absorption spectra contain two main features: X-ray absorption near edge structure (XANES) and extended X-ray absorption fine structure (EXAFS). Information that can be deduced from XANES includes oxidation states and valence shell electron population [63]. The XANES technique was practiced in our study to determine the oxidation states and d-electron density of metals in the catalysts.

3.5.1. Oxidation states of Ce

Fig. 5(a) shows XANES spectra recorded at the Ce L_3 edge for standards $Ce(NO_3)_3{\cdot}6H_2O$, CeO_2, 1%Re/CeO_2 and 5%Co/CeO_2. It is clearly seen that XANES spectra of standard $Ce(NO_3)_3{\cdot}6H_2O$ exhibits a single white line at 5725.5 eV. This peak characterizes the Ce in the trivalent state and the transition was labeled as dipole allowed transition of Ce 2p to Ce 4f ^{1}5d final state [64]. For Ce in the tetravalent state (CeO_2) a double white line is usually observed. These two peaks were assigned as transitions of Ce 2p to a mixed valance state of cerium, one with ground state electronic configuration $4f^0$ and another with $4f^1$ [65]. Apart from 2 major peaks A and B, a small low-energy shoulder (c) and a pledge peak (D) are usually observed for CeO_2. The lower energy shoulder was due to the crystal field splitting of the Ce 5d state for bulk CeO_2 or is assigned to a Ce^{3+} impurity [64]. The feature D was assigned to the dipole forbidden $2p_{3/2} \rightarrow 4f$ transition or a transition to the unoccupied Ce d state at the bottom of the CeO_2 conduction band [66]. Our XANES spectra of 1%Re/CeO_2, 5%Co/CeO_2 display features that are similar to those of CeO_2.

The jump in energy in XANES spectra indicates energy that is required to raise electrons up from core level to unoccupied valence band and it is called the edge energy. The edge energy can be accurately derived by differentiating the XANES spectra and assigning the turning point of the derivative spectra as the edge energy. Various investigators have found a relationship between metal oxidation states and the energy shifts of the absorption edge [31,67]. The Ce L_3 edge energy shifts of 1%Re/CeO_2, 5%Co/CeO_2, 1%Re–5%Co/CeO_2, $Ce(NO_3)_3{\cdot}6H_2O$ and CeO_2 were plotted relative to the edge energy of Ce^0 in Fig. 5(b). A linear fit was constructed through L_3 energy shifts of Ce^0, Ce^{3+} and Ce^{4+}. The edge energy shifts of 5%Co/CeO_2, 1%Re/CeO_2, and 1%Re–5%Co/CeO_2 relative to Ce^0 was placed on this straight line at appropriate ΔE and the apparent oxidation states of Ce of these compounds lay between +3 and +4. The result indicates the coexistence of Ce^{3+} and Ce^{4+} in which Co reduced surface Ce^{4+} in CeO_2 by transferring electron density into d-orbitals of Ce^{4+}, leading to a small amount of Ce^{3+}. Evidence that electrons were transferred from Co^{2+} will be shown by increases of Co oxidation states in the next section. Among these three catalysts, the oxidation state of Ce in 1%Re–5%Co/CeO_2 was the lowest. This result seems to indicate that Re assists Co in reducing Ce^{4+} giving rise to more Ce^{3+}at the surface of the ceria support.

3.5.2. Oxidation states of Co and Re

The plot of XANES spectra and the edge energy shift of Co^{2+} and Co^{3+} (K absorption edge) relative to the edge energy of Co^0 are displayed in Fig. 6. A linear fit was constructed through K edge energy shift of Co^0, Co^{2+} and Co^{3+} in Fig. 6(b). The edge energy shifts of 10%Co/CeO_2, 1%Re–10%Co/CeO_2 and 10%Re–10%Co/CeO_2 when placed on this straight line indicate that the oxidation state of Co in these compounds lies above +2. For 10%Co/CeO_2, the oxidation state of Co appears to be ~+2.1. Together with the result from Fig. 5(b) it can be concluded that electron density was transferred from Co^{2+} to Ce^{4+} leading to increase in oxidation state of Co^{2+} and lowering of oxidation state of Ce^{4+}. For 1%Re–10%Co/CeO_2, the oxidation state of Co^{2+} is found to further increase to ~+2.7. This result indicates that Co^{2+} also donates some electrons to Re leading to further increase in its oxidation state. With higher content of Re (10%Re) further increase in Co oxidation state was observed. From these results we can conclude that Co^{2+} donates its electron to both Ce^{4+} and Re^{7+}.

Fig. 7 shows XANES spectra and a plot of edge energy shift of Re M_5 absorption edges for 1%Re–10%Co/CeO_2, 1%Re–20%Co/CeO_2 and 1%Re/CeO_2 as compared to Re^0 powder and Re^{7+} in NH_4ReO_4. A linear fit was constructed through M_5 energy shift of Re^0 and Re^{7+}. Although only two standards (Re^0 and Re^{7+}) were used in this study, we are confident in drawing a straight line for edge energy shift of these two standards since many papers have reported a linear correlation between Re valence and its chemical shift with respect to metallic Re [30,31]. The edge energy shift of 1%Re–10%Co/CeO_2, and 1%Re–20%Co/CeO_2, when placed on this straight line, indicates the oxidation state of Re to be a little above +6 while the oxidation

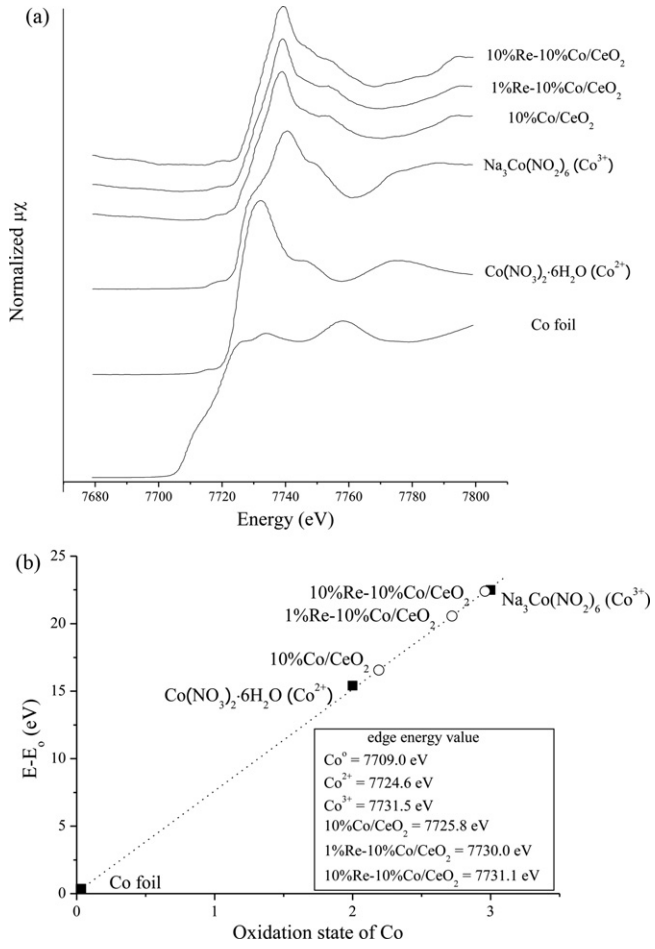

Fig. 6. (a) XANES spectra of the Co K absorption edge for Co foil (Co^0), $Co(NO_3)_2{\cdot}6H_2O$ (Co^{2+}), $Na_3Co(NO_2)_6$ (Co^{3+}), $10\%Co/CeO_2$, $1\%Re–10\%Co/CeO_2$ and $10\%Re–10\%Co/CeO_2$. (b) Relationship between edge energy shift of Co compounds and the oxidation states. Filled squares are Co^0, $Co(NO_3)_3{\cdot}6H_2O$ (Co^{2+}) and $Na_3Co(NO_2)_6$ (Co^{3+}) standards, open circles are $10\%Co/CeO_2$, $1\%Re–10\%Co/CeO_2$ and $10\%Re–10\%Co/CeO_2$.

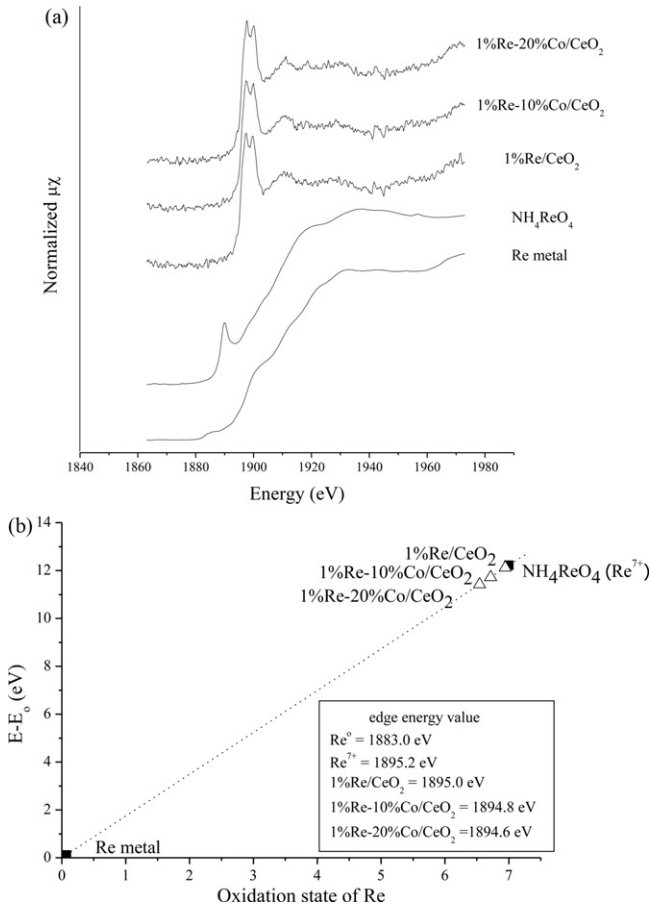

Fig. 7. (a) XANES spectra of the Re M_5 absorption edge for Re metal (Re^0), NH_4ReO_4 (Re^{7+}), $1\%Re/CeO_2$, $1\%Re–10\%Co/CeO_2$ and $1\%Re–20\%Co/CeO_2$. (b) Relationship between edge energy shift of Re compounds and the oxidation states. Filled squares are Re powder (Re^0) and NH_4ReO_4 (Re^{7+}) standard, open triangles are $1\%Re/CeO_2$, $1\%Re–10\%Co/CeO_2$ and $1\%Re–20\%Co/CeO_2$.

state of Re in $1\%Re/CeO_2$ was +7. Lowering of Re oxidation state in bimetallic $Re–Co/CeO_2$ indicates movement of electron density into the d-state of Re.

Study of oxidation states of all metals in the catalysts seems to indicate that Co^{2+} donates electron density to both CeO_2 and Re in the catalysts, leading to a higher oxidation state of cobalt and lowering of rhenium and cerium oxidation states.

3.5.3. *The role of Re in enhancing WGS activity*

To further confirm the direction of electron movement among the metals in the catalysts, the white line intensities of Re and Co in the catalysts were compared. The intensity of the white line is related to occupancy of the d-state of the element. A highly occupied d-state means that fewer core electrons can be excited into its d-state, therefore the intensity of the absorption peak is low. Oppositely, if the d-state is only slightly occupied, more core electrons can be excited and move into it, and so the absorption peak is strong. In comparison, higher white line intensity indicates lower electron density in d-states. Fig. 8(a) compares white line intensity of Re M_5 absorption for 1%Re in the vicinity of 10% and 20%Co. In this figure, the white line intensity of 1%Re with 10%Co is a little higher than that of 20%Co which indicates that Re in the vicinity of 10%Co has less d-electrons than Re with 20%Co. The result indicates that 10%Co donates less d-electrons to Re than 20%Co. On the contrary, Fig. 8(b) illustrates the white line intensity of Co K absorption for 10%Co in the vicinity of 1%Re and 10%Re. The higher peak belongs to 10%Re, which also indicates that Co with 10%Re has less d-electrons than Co with 1%Re. This result indicates that higher content of Re withdraws more electrons from Co. A catalyst with higher content of Re withdraws more electrons from Co than a catalyst with less content of Re. Therefore, electron movement from Co to Re is confirmed. The XANES spectra of Re in Fig. 8(a) contains rather high background due to limitations of the instrument. The source energy was low and Re absorption was taken at the M_5 absorption edge. However, six spectra were averaged and care was taken in placing the pre-edge and post-edge of the spectra at the same position. Although the differences of the white line intensities were low, the direction of electron density transfer indicated by the white line intensities corresponds well with the information obtained from Figs. 6 and 7.

The results from oxidation states and white line intensity comparison for both Re and Co in the catalyst tend to indicate that electron densities are transferred from Co to Re d-orbital, giving rise to lowering of Re oxidation state and increasing of electron density in Re d-states. The role of Re in enhancing WGS activity of $Re–Co/CeO_2$ can be explained by the electron withdrawing effect of Re. As a result of the electron withdrawing effect of Re, the d-electrons density of Co are partially transferred to the d-orbital of Re, and so the d-electrons density of Co that are available for back donation to the π^* orbital of adsorbed CO are less, the Co-adsorbate bonds are weaker and the CO_2 product can easily leave the catalyst surface. Apart from an electron withdrawing effect of

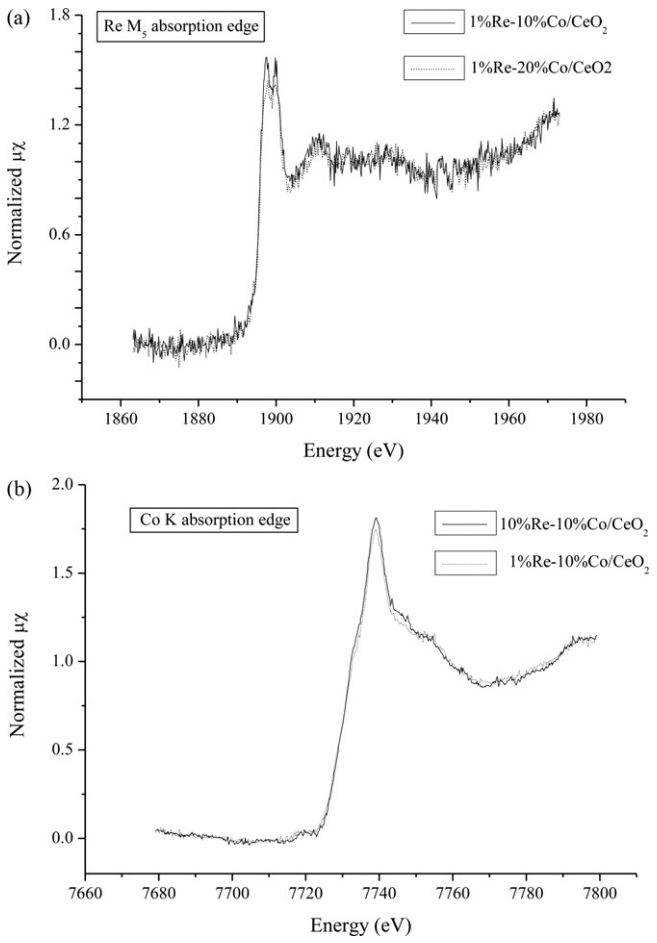

Fig. 8. (a) Comparison of white line intensity of Re M_5 absorption edge for1%Re–10%Co/CeO_2 and 1%Re–20%Co/CeO_2. (b) Comparison of white line intensity of Co absorption edge for 1%Re–10%Co/CeO_2 and 10%Re–10%Co/CeO_2.

Re, H_2-chemisorption study also displays that Re increases the Co dispersion on the ceria support and the active sites available for WGS reaction increase.

Another factor that may be of more importance is the effect that Re contributes to reduction of Ce^{4+} to Ce^{3+}. The presence of Ce_2O_3 at the ceria surface gives rise to oxygen vacancies which facilitate the electron movement at the surface leading to ease of surface reduction. This result agrees with the TPR results that display surface reduction peaks at a temperature lower than the ceria surface reduction temperature of 520 °C. Many papers have reported that the WGS mechanism involves the redox mechanism on the ceria surface [1,6,68]. The major role of Re in enhancing the WGS activity of Co/CeO_2 may be the ability to promote the reduction of the ceria surface leading to lowering of reduction temperature, increased oxygen vacancies, and increased surface redox property.

4. Conclusion

The catalytic activities of Re–Co/CeO_2 bimetallic catalysts for WGS reaction were investigated and the results show that the WGS reaction rate provided by Re–Co/CeO_2 was much higher than the rate provided by Co/CeO_2. XRD and Raman spectroscopy results indicate that metal oxides were dispersed on ceria surface and H_2-chemisorption indicated better dispersion of Co on the ceria surface upon addition of Re. H_2-TPR results reveal that doping of Re onto Co/CeO_2 to form Re–Co/CeO_2 bimetallic catalysts leads to lowering of surface reduction temperature. The effect of Re on enhancing the catalytic activity for the WGS reaction was described by XANES. The XANES spectra of Ce L_3 absorption edge indicates the presence of Ce_2O_3 which produces oxygen vacancies. The XANES spectra of Re M_5 and Co K absorption edges and white line comparison indicate that Re withdraws electron density from Co and lowers the back-donation of d-electron from cobalt to π^* orbital of adsorbed CO molecules. In conclusion, it seems that Re influences the catalysts and the catalyst performance in several ways. Re increases the reducibility of the surface ceria, and facilitates the redox process at the surface. Re also increases the metal active sites and weakens the active metal-adsorbate bonds. All of these effects contribute to an increase in the WGS reaction rates.

Acknowledgements

The authors would like to thank the Center of Excellence for Innovation in Chemistry (PERCH-CIC), Commission on Higher Education, Ministry of Education and the National Nanotechnology Center, National Science and Technology Development Agency for financial support. Generous beam time from the Synchrotron Light Research Institute (SLRI) is gratefully acknowledged.

References

[1] R.J. Gorte, S. Zhao, Catal. Today 104 (2005) 18–24.
[2] S. Hilaire, X. Wang, T. Luo, R.J. Gorte, J. Wagner, Appl. Catal. A: Gen. 258 (2004) 271–276.
[3] X. Qi, M. Flytzani-Stephanopoulos, Ind. Eng. Chem. Res. 43 (2004) 3055–3062.
[4] M. Asadullah, K. Fujimoto, K. Tomishige, Ind. Eng. Chem. Res. 40 (2001) 5894–5900.
[5] L. Kundakovic, M. Flytzani-Stephanopoulos, J. Catal. 179 (1998) 203–221.
[6] G. Jacobs, E. Chenu, P.M. Patterson, L. Williams, D. Sparks, G. Thomas, B.H. Davis, Appl. Catal. A: Gen. 258 (2004) 203–214.
[7] E. Mamontov, T. Egami, R. Brezny, M. Koranne, S. Tyagi, J. Phys. Chem. B 104 (2000) 11110–11116.
[8] H. Cordatos, T. Bunluesin, J. Stubenrauch, J.M. Vohs, R.J. Gorte, J. Phys. Chem. 100 (1996) 785–789.
[9] A.D. Mayernick, M.J. Janik, J. Phys. Chem. C 112 (2008) 14955–14964.
[10] A. Martnez-Arias, M. Fernndez-Garca, L.N. Salamanca, R.X. Valenzuela, J.C. Conesa, J. Soria, J. Phys. Chem. B 104 (2000) 4038–4046.
[11] T. Kim, J.M. Vohs, R.J. Gorte, Ind. Eng. Chem. Res. 45 (2006) 5561–5565.
[12] A. Martnez-Arias, J.M. Coronado, R. Catalua, J.C. Conesa, J. Soria, J. Phys. Chem. B 102 (1998) 4357–4365.
[13] P. Bera, A. Gayen, M.S. Hegde, N.P. Lalla, L. Spadaro, F. Frusteri, F. Arena, J. Phys. Chem. B 107 (2003) 6122–6130.
[14] X. Wang, R.J. Gorte, Appl. Catal. A: Gen. 247 (2003) 157–162.
[15] S.H. Oh, G.B. Hoflund, J. Phys. Chem. A 110 (2006) 7609–7613.
[16] J. Zhou, D.R. Mullins, J. Phys. Chem. B 110 (2006) 15994–16002.
[17] A. Gayen, K.R. Priolkar, P.R. Sarode, V. Jayaram, M.S. Hegde, G.N. Subbanna, S. Emura, Chem. Mater. 16 (2004) 2317–2328.
[18] T. Utaka, T. Okanishi, T. Takeguchi, R. Kikuchi, K. Eguchi, Appl. Catal. A: Gen. 245 (2003) 343–351.
[19] A. Basińska, K. Pawełczyk, React. Kinet. Catal. Lett. 89 (2006) 325–331.
[20] V. Idakiev, T. Tabakova, A. Naydenov, Z.Y. Yuan, B.L. Su, Appl. Catal. B: Environ. 63 (2006) 178–186.
[21] W. Deng, A.I. Frenkel, R. Si, M. Flytzani-Stephanopoulos, J. Phys. Chem. C 112 (2008) 12834–12840.
[22] A.M. Duarte de Farias, P. Bargiela, M.G.C. Rocha, M.A. Fraga, J. Catal. 260 (2008) 93–102.
[23] S.Y. Choung, M. Ferrandon, T. Krause, Catal. Today 99 (2005) 257–262.
[24] R. Radhakrishnan, R.R. Willigan, Z. Dardas, T.H. Vanderspurt, Appl. Catal. B: Environ. 66 (2006) 23–28.
[25] H. Iida, A. Igarashi, Appl. Catal. A: Gen. 303 (2006) 192–198.
[26] A. Venugopal, J. Aluha, M.S. Scurrell, Catal. Lett. 90 (2003) 1–6.
[27] P. Marques, N.F.P. Ribeiro, M. Schmal, D.A.G. Aranda, M.M.V.M. Souza, J. Power Sources 158 (2006) 504–508.
[28] A. Katayama, J. Phys. Chem. 84 (1980) 376–381.
[29] G.M. Bickle, J.N. Beltramini, D.D. Do, Ind. Eng. Chem. Res. 29 (1990) 1801–1807.
[30] E.L. Kunkes, D.A. Simonetti, J.A. Dumesic, W.D. Pyrz, L.E. Murillo, J.G. Chen, D.J. Buttrey, J. Catal. 260 (2008) 164–177.
[31] F. Hilbrig, C. Michel, G.L. Haller, J. Phys. Chem. 96 (1992) 9893–9899.
[32] A. Jentys, B.J. McHugh, G.L. Haller, J.A. Lercher, J. Phys. Chem. 96 (1992) 1324–1328.
[33] D.C. Huang, K.H. Chang, W.F. Pong, P.K. Tseng, K.J. Hung, W.F. Huang, Catal. Lett. 53 (1998) 155–159.
[34] L.G.S. Pereira, V.A. Paganin, E.A. Ticianelli, Electrochim. Acta 54 (2009) 1992–1998.
[35] G. Jacobs, J.A. Chaney, P.M. Patterson, T.K. Das, B.H. Davis, Appl. Catal. A: Gen. 264 (2004) 203–212.

[36] Y. Li, Q. Fu, M. Flytzani-Stephanopoulos, Appl. Catal. B: Environ. 27 (2000) 179–191.
[37] X. Wang, J.A. Rodriguez, J.C. Hanson, D. Gamarra, A. Martıínez-Arias, M. Fernandez-Garcıa, J. Phys. Chem. B 110 (2006) 428–434.
[38] T. Tabakova, V. Idakiev, J. Papavasiliou, G. Avgouropoulos, T. Ioannides, Catal. Commun. 8 (2007) 101–106.
[39] M.G. Sanchez, J.L. Gazquez, J. Catal. 104 (1987) 120–135.
[40] P. Panagiotopoulou, J. Papavasiliou, G. Avgouropoulos, T. Ioannides, D.I. Kondarides, Chem. Eng. J. 134 (2007) 16–22.
[41] E.S. Bickford, S. Velu, C. Song, Catal. Today 99 (2005) 347–357.
[42] W. Klysubun, P. Sombunchoo, N. Wongprachanukul, P. Tarawarakarn, S. Klinkhieo, J. Chaiprapa, P. Songsiriritthigul, Nucl. Instrum. Meth. Phys. Res. A 582 (2007) 87–89.
[43] Y. Sato, Y. Soma, T. Miyao, S. Naito, Appl. Catal. A: Gen. 304 (2006) 78–85.
[44] W. Cai, F. Wang, E. Zhan, A.C.V. Veen, C. Mirodatos, W. Shen, J. Catal. 257 (2008) 96–107.
[45] Q. Fu, W. Deng, H. Saltsburg, M. Flytzani-Stephanopoulos, Appl. Catal. B: Environ. 56 (2005) 57–68.
[46] X. Wu, J. Fan, R. Ran, D. Weng, Chem. Eng. J. 109 (2005) 133–139.
[47] Q. Fu, A. Weber, M. Flytzani-Stephanopoulos, Catal. Lett. 77 (2001) 87–95.
[48] R.D. Monte, J. Kaspar, J. Mater. Chem. 15 (2005) 633–648.
[49] V.G. Keramidas, W.B. white, J. Chem. Phys. 59 (1973) 1561–1562.
[50] J.R. McBride, K.C. Hass, B.D. Poindexter, W.H. Weber, J. Appl. Phys. 76 (1994) 2435–2441.
[51] I. Zacharaki, C.G. Kontoyannis, S. Boghosian, A. Lycourghiotis, Ch. Kordulis, Catal. Today 143 (2009) 38–44.
[52] D. Gallant, M. Pzolet, S. Simard, J. Phys. Chem. B 110 (2006) 6871–6880.
[53] G.L. Markaryan, L.N. Ikryannikova, G.P. Muravieva, A.O. Turakulova, B.G. Kostyuk, E.V. Lunina, V.V. Lunin, E. Zhilinskaya, A. Aboukais, Colloids Surf. A: Physicochem. Eng. Aspects 151 (1999) 435–447.
[54] Y. Yuan, Y. Iwasawa, J. Phys. Chem. B 106 (2002) 4441–4449.
[55] M.F.L. Johnson, V.M. LeRoy, J. Catal. 35 (1974) 434–440.
[56] A.N. Webb, J. Catal. 39 (1975) 485–486.
[57] J.Y. Luo, M. Meng, X. Li, X.G. Li, Y.Q. Zha, T.D. Hu, Y.N. Xie, J. Zhang, J. Catal. 254 (2008) 310–324.
[58] T.K. Das, G. Jacobs, P.M. Patterson, W.A. Conner, J. Li, B.H. Davis, Fuel 82 (2003) 805–815.
[59] C.L. Pieck, M.B. González, J.M. Parera, Appl. Catal. A: Gen. 205 (2001) 305–312.
[60] L.F. Liotta, G. Di Carlo, G. Pantaleo, A.M. Venezia, G. Deganello, Appl. Catal. B: Environ. 66 (2006) 217–227.
[61] O. Thinon, F. Diehl, P. Avenier, Y. Schuurman, Catal. Today 137 (2008) 29–35.
[62] A.A. Phatak, N. Koryabkina, S. Rai, J.L. Ratta, W. Ruettinger, R.J. Farrauto, G.E. Blau, W.N. Delgass, F.H. Ribeiro, Catal. Today 123 (2007) 224–234.
[63] Y. Iwasawa (Ed.), X-ray Absorption Fine Structure for Catalysts and Surfaces, World Scientific Publishing, Singapore, 1995, p. 60.
[64] J. Zhang, X. Ju, Z.Y. Wu, T. Liu, T.D. Hu, Y.N. Xie, Chem. Mater. 13 (2001) 4192–4197.
[65] A.M. Shahin, F. Grandjean, G.J. Long, T.P. Schuman, Chem. Mater. 17 (2005) 315–321.
[66] P. Nachimuthu, W.C. Shih, R.S. Liu, L.Y. Jang, J.M. Chen, J. Solid State Chem. 149 (2000) 408–413.
[67] T. Ressler, J. Wienold, R.E. Jentoft, T. Neisius, J. Catal. 210 (2002) 67–83.
[68] S. Hilaire, X. Wang, T. Luo, R.J. Gorte, J. Wagner, Appl. Catal. A: Gen. 215 (2001) 271–278.